Anisotropic deformation response of single protein molecules

Hendrik Dietz, Felix Berkemeier, Morten Bertz, and Matthias Rief†

Physik Department E22, Technische Universität München, James-Franck-Strasse, D-85748 Garching, Germany

Edited by Ronald D. Vale, University of California, San Francisco, CA, and approved July 6, 2006 (received for review April 12, 2006)

Single-molecule methods have given experimental access to the mechanical properties of single protein molecules. So far, access has been limited to mostly one spatial direction of force application. Here, we report single-molecule experiments that explore the mechanical properties of a folded protein structure in precisely controlled directions by applying force to selected amino acid pairs. We investigated the deformation response of GFP in five selected directions. We found fracture forces widely varying from 100 pN up to 600 pN. We show that straining the GFP structure in one of the five directions induces partial fracture of the protein into a half-folded intermediate structure. From potential widths we estimated directional spring constants of the GFP structure and found values ranging from 1 N/m up to 17 N/m. Our results show that classical continuum mechanics and simple mechanistic models fail to describe the complex mechanics of the GFP protein structure and offer insights into the mechanical design of protein materials.

cysteine engineering | GFP | protein mechanics | protein stability | single-molecule force spectroscopy

Many processes in living systems, such as cell division, locomotion, and enzyme activity, depend critically on single protein molecule properties like mechanical rigidity or conformational changes (1, 2). The invention of single-molecule manipulation techniques has given experimental access to the mechanical properties of soluble protein molecules (3–8) and membrane proteins (9–12). Current recombinant protein expression naturally links individual protein modules by their N and C termini. Experimental access to the deformation response of proteins has, thus, so far been limited almost exclusively to one direction of force application: the N- to C-terminal linkage direction of polyproteins. Previous experiments with two proteins that naturally exhibit a non-N- to C-terminal linkage have indicated that the mechanics of protein structures depend on loading geometry (13, 14). Theoretical studies have predicted that the deformation response of proteins may vary largely, even on the single-residue level, and that protein structures may contain "soft" and "stiff" regions (15). In this study, we employ cysteine engineering (16) to gain precise control over the points of force application to a single protein structure.

Fig. 1 illustrates the quality of information that controlled force application can supply about the mechanics of a single protein. Fracture or unfolding of a protein structure proceeds on a high-dimensional energy surface determined by multiple weak interactions between amino acid residues (17). Such an energy landscape is schematically shown in Fig. 1. Conventional N- to C-terminal linkage mechanically probes only a single direction (e.g., pathway I in Fig. 1). In turn, complete control of linkage topology makes previously hidden regions of the energy landscape accessible. Directions in which the protein appears soft and fractures easily will be characterized by low- and shallow-energy barriers in this landscape (Fig. 1, pathway I), whereas directions with high stability and stiff spring constants will exhibit large and steep barriers (Fig. 1, pathway II). Mechanical exploration of hidden regions of the energy landscape may even lead to the creation of intermediate structures (Fig. 1, pathway III) that appear when the protein structure fractures only partially.

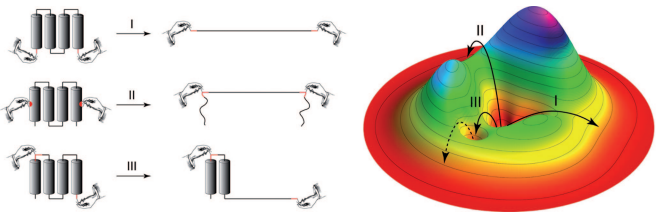

Fig. 1. Probing single-protein stability in different directions of force application. The application of force to selected amino acid pairs in a folded protein structure can sample different pathways (I–III) in a protein's free-energy surface. Directed force application yields the protein's directional deformation response and may even control the population of hidden local energy minima, corresponding to partially folded protein structures (pathway III).

Results and Discussion

In the current study, we chose GFP to explore the three-dimensional deformation response and mechanical stability of a prominent protein structure motif. The β-barrel structure of the GFP-like fold (18) is commonly considered extremely stable (19–21). Surprisingly, previous experiments loading single GFP molecules in the conventional N- to C-terminal direction revealed very low mechanical stability (22) compared with other β-sheet protein structures, like the muscle protein titin (23, 24). By introducing two cysteine residues at the desired linkage points, we constructed disulfide-linked polyprotein chains (16) with five particular linkage geometries (see Fig. 2*a*). The spatial positions of the linking cysteines in the folded tertiary structure define the points of force application to the molecule (Fig. 2*a*) when single polyprotein chains are stretched between cantilever tip and surface of an atomic force microscope. Double-cysteine-based polymerization does not control the direction of inclusion of individual modules in the polymerized protein chain. Because of inversion symmetry in the geometry of force application, this freedom in the molecular construction has no influence on force-extension data. Fig. 2*b* displays typical force-extension traces recorded with each of the five differently linked GFP polymers. Full-scale traces and additional data are provided in the supporting information, which is published on the PNAS web site. The traces in Fig. 2*b* are overlaid with a lattice of calculated worm-like chain (WLC) curves. The spacing between the WLC curves corresponds to the gain in contour length expected from the unfolding of a single GFP molecule along the respective linkage geometry (16). It becomes obvious that each peak reflects the forced fracture of a single GFP structure along the direction defined by the linking amino acids, followed by elon-

Conflict of interest statement: No conflicts declared.

This paper was submitted directly (Track II) to the PNAS office.

Abbreviation: WLC, worm-like chain.

†To whom correspondence should be addressed. E-mail: mrief@ph.tum.de.

www.pnas.org/cgi/doi/10.1073/pnas.0602995103

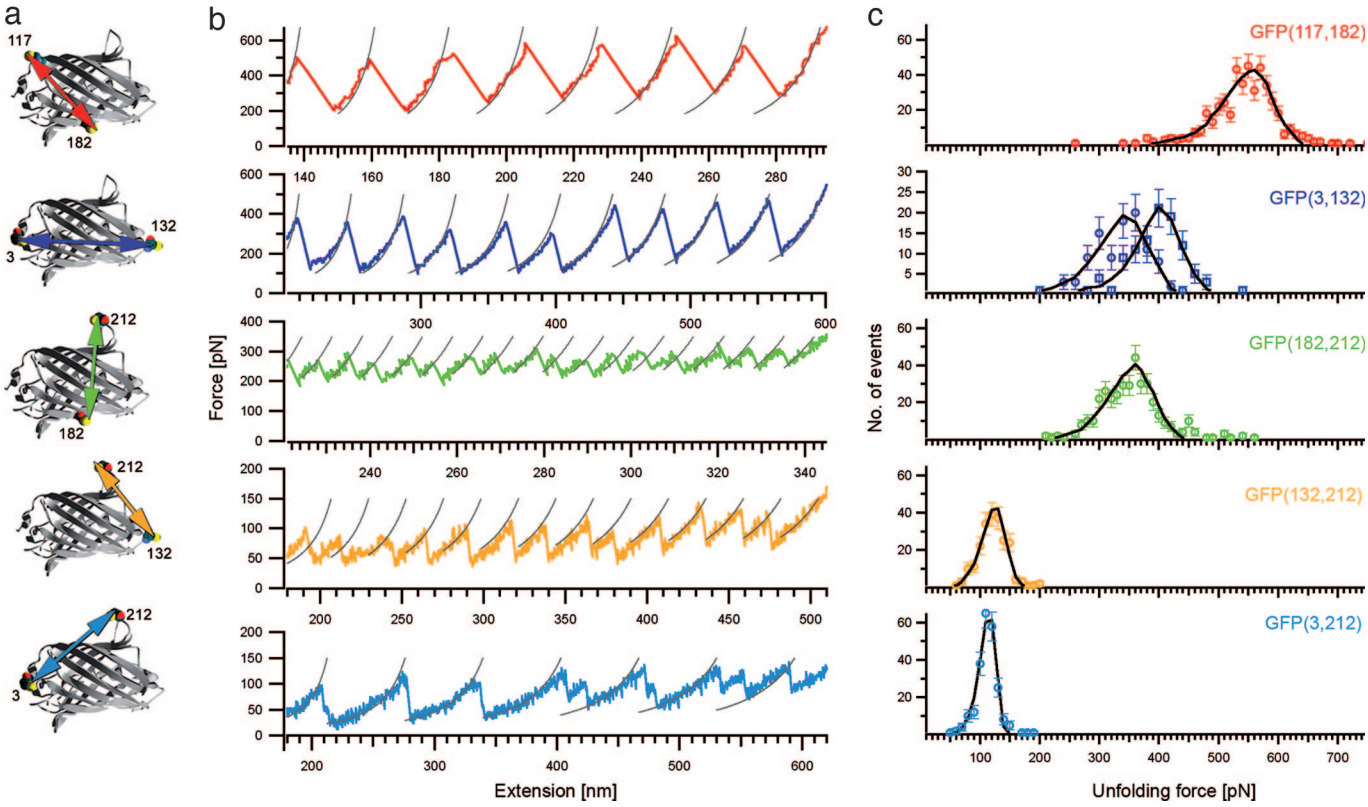

Fig. 2. Exploring the directional deformation response of GFP. (*a*) Location of cysteine mutations in GFP (space-filled residues) that define the points and direction of force application to an individual GFP monomer in GFP polyproteins. (*b*) Typical single-molecule force-extension traces obtained with the differently linked GFP polyproteins. See the supporting information for full-scale traces and additional data. (*c*) Experimental (circles) and Monte-Carlo-simulated (black solid lines) fracture force distributions. Error bars are calculated by taking the square root of the number of events. For GFP(3, 132), we measured and simulated fracture force distributions at two different pulling speeds (circles, 2 μm/s; squares, 12 μm/s).

gation of the lengthened polypeptide chain. Additional evidence showing the single-molecule nature of our data is provided in the supporting information.

One possible concern is whether the individual unfolding events truly reflect the properties of individual, nonperturbed GFP molecules. External contributions, such as interface interaction between neighboring protein domains, may arise in multimeric proteins (25). Yet all cysteine-mutated GFP solutions in the initial, nonpolymerized state and in the polymerized state displayed the typical bright fluorescence, corroborating directly the intact and correctly folded molecular protein structure (19). Another important piece of evidence against protein interface interactions influencing single-module unfolding events comes from the observation that the individual GFP modules in the chain behave statistically independent when subject to a force. Consistently, on average, the first unfolding events in our polyproteins occur at lower forces than the last events (see Fig. 2*b*; see also the supporting information). This effect can be understood by considering that, for the first unfolding events, many modules are polled in parallel. The number of still-folded modules increases the effective unfolding rate (26, 27). In turn, for the last events, only few modules can unfold. If, on the other hand, interactions between the modules would take place, one would expect the force of the last unfolding events to be considerably below the previous ones, which we do not observe.

Directional Mechanical Stability of a Folded Protein Structure. Fig. 2*c* displays the fracture force distributions for the unfolding of single GFP molecules along the five force-loading geometries. The most striking result is the large variation in fracture force among the different directions. Forces span the whole range from almost 600 pN for the direction (117, 182) down to 100 pN for the direction (3, 212). 600 pN is the highest force ever reported for breaking noncovalent molecular structures and is not far from rupturing covalent bonds [1.5 nN (28)]. The variation in stability becomes even more drastic taking into account that GFP when loaded along the N- to C-terminal direction starts to fracture already at forces $\approx$35 pN in a loading-rate-independent equilibrium process (22). Beyond a simple stability analysis, the force-extension data also supplies insights into transition barrier heights and positions (29). Monte Carlo simulations of the unfolding force distributions of Fig. 2*c* yielded barrier heights and potential widths in the protein's energy landscape as shown in Table 1. Interestingly, barrier heights do not vary significantly along the different directions of force application. In contrast, the most prominent effect is a large variation in potential width. The most stable direction (117, 182) exhibits a potential width of only 0.12 nm, indicating a very steep potential and, thus, a large mechanical stiffness (see Fig. 1, pathway II). In contrast, the weakest direction (3, 212) exhibits a shallow potential width of 0.45 nm, corresponding to a much greater mechanical compliance (compared with pathway I in Fig. 1).

Directional Spring Constants of a Folded Protein Structure. The potential widths extracted from our experiments are a measure for the mechanical properties of the fracture interface within the protein structure. In the simplest possible model, we can extract from these numbers information about directional molecular spring constants (see *Materials and Methods* and ref. 30). In this model, we assume that the energy profile has parabolic shape

Table 1. Directional mechanical stability, elasticity, and kinetic parameters of the GFP structure

Direction of load (i, j)	Average fracture force, pN (speed, μm/s)	Potential width $\Delta x_{i,j}$, nm	Barrier height $\Delta G^{*}_{i,j} \pm 2$, k_BT	Unloaded transition rate $k_{i,j}$, 1/s	Directional spring constant $p_{i,j}$, N/m
(117, 182)	548 ± 57 (3.6)	0.12 ± 0.003	31	$5{\cdot}10^{-5} \pm 4{\cdot}10^{-5}$	17
(3, 132)	407 ± 45 (12)	0.125 ± 0.005	26	$4{\cdot}10^{-3} \pm 3{\cdot}10^{-3}$	13
(3, 132)	346 ± 46 (2)	0.125 ± 0.004	26	$4{\cdot}10^{-3} \pm 3{\cdot}10^{-3}$	13
(182, 212)	356 ± 61 (3.6)	0.14 ± 0.002	27	$2.2{\cdot}10^{-3} \pm 8{\cdot}10^{-4}$	11
(132, 212)	127 ± 23 (3.6)	0.32 ± 0.005	26	$5{\cdot}10^{-3} \pm 3{\cdot}10^{-3}$	2
(3, 212)	117 ± 19 (3.6)	0.45 ± 0.006	28	$4{\cdot}10^{-4} \pm 2{\cdot}10^{-4}$	1
(132, 212)†	117 ± 22 (3.6)	0.32 ± 0.015	25	$14{\cdot}10^{-3} \pm 7{\cdot}10^{-3}$	2
(3, 212)†	115 ± 22 (3.6)	0.45 ± 0.01	28	$8{\cdot}10^{-4} \pm 1.4{\cdot}10^{-3}$	1

The slightly less average fracture force of (132, 212)-linked GFP in the copolymer can be attributed to the lower effective loading rate in the copolymer. Errors in potential width and unloaded transition rate are the statistical fitting errors.
†Obtained from GFP(3, 212)(132, 212) copolymers.

and, hence, that its curvature does not change with applied force. The spring constant will then be the curvature of the energy profile. This assumption need not hold true over the whole force range. Nevertheless, such numbers can give more intuitive information about the mechanical properties of the folded protein molecule under load. The directional molecular spring constants calculated under the above assumptions vary from 1 N/m for (3, 212) to 17 N/m for (117, 182) (Table 1). The directional deformation response of GFP is visualized in Fig. 3. Average fracture forces are given by the width of the strings connecting the points of force application, whereas the color of the strings codes for the directional spring constants.

Fig. 3 manifests the complexity of single-protein mechanics. Any continuum mechanical modeling of the GFP barrel would fail to describe the large directional variation in both rupture forces and spring constants. Instead, the drastic directional stability changes within the protein structure reflect its grainy composition. It becomes evident that stability of the structure is not simply determined by mere detachment of the amino acids at the points of force application. An example is residue 212. Although this residue is involved in the linkage geometries with the lowest rupture forces and, therefore, may appear as a weak site, in GFP(182, 212) it still can resist much higher forces. Another example is residue 3, which resides in an α-helical region previously classified as mechanically labile (22) with detachment forces of 35 pN. If pulled in direction (3, 132), residue 3 surprisingly exhibits unfolding forces as large as 400 pN. Obviously the fracture lines within the protein and the transition state structures differ considerably among the various linkage geometries. Because simple mechanistic models fail, future full molecular dynamics simulations (31, 32) will have to explain this host of data now accessible from single-molecule experiments.

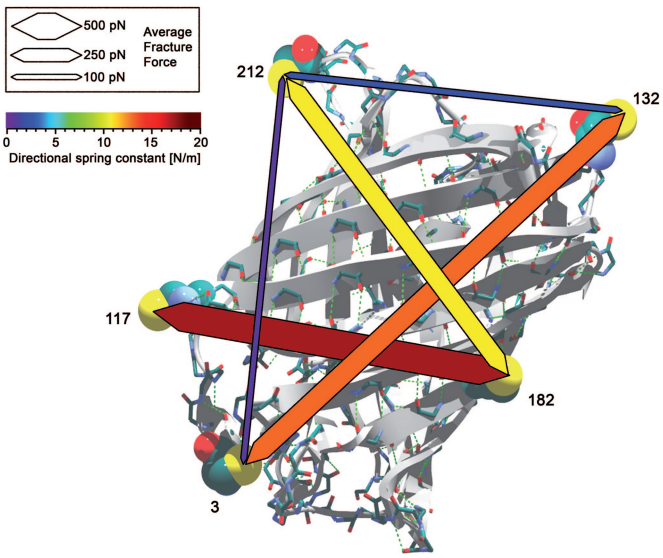

Fig. 3. Directional deformation response of the GFP fold. The width of the strings connecting points of force application (space-filled residues) represents the average fracture force in that particular direction. The color of the strings encodes the directional spring constant, i.e., protein rigidity in the respective direction. The GFP structure was drawn with ID code 1EMB (38) from the Protein Data Bank one-dimensional file.

Selective Population of Local Minima in a Protein's Free-Energy Surface. An interesting aspect of mechanical linkage control becomes apparent in the force-extension traces of GFP when loaded along (3, 212). A sample trace is shown in Fig. 4*a*. Although, in all other deformation directions examined here, the application of force induces a single all-or-none fracture event in which the complete loaded protein structure unfolds, GFP(3, 212) exhibits an unfolding intermediate. Two classes of fracture events of GFP(3, 212) can be observed: complete unfolding without population of an intermediate (Fig. 4*a*, marked in blue) and unfolding into an intermediate structure (Fig. 4*a*, marked in red), followed by unfolding of the intermediate (Fig. 4*a*, marked in green). A histogram of contour length increases as determined by WLC fits to individual peaks in single-molecule force-extension traces is shown in Fig. 4*b*. Clear peaks at 32.8 nm for the transition to the intermediate, at 39.3 nm for intermediate unfolding, and at 72.08 nm for complete unfolding can be observed. The sum of the two shorter lengths matches the length for complete unfolding within 2 Å, supporting a scheme with two parallel unfolding pathways. An alternative explanation assuming a single pathway where the blue class of events would correspond to a missed detection of the intermediate state can be ruled out, given the significant fraction of complete unfolding events lacking any signs of an intermediate structure down to a time scale of 300 μs.

The force distributions shown in Fig. 4*c* exhibit similar average forces and widths for both pathways (blue and red), albeit with different population frequencies. There are two possible explanations for these similar widths: Either the protein unfolds via two separate transition barriers that then must be quite similar both in potential width and in barrier height, or the narrow distribution might be an indication that the bifurcation into two pathways occurs after the major transition state, which could be identical for both pathways. Interface stabilization of neighboring domains also could be a potential source for an apparent two-pathway behavior, as observed for fracture of GFP along the (3, 212) direction. In such a case, the frequency of partial

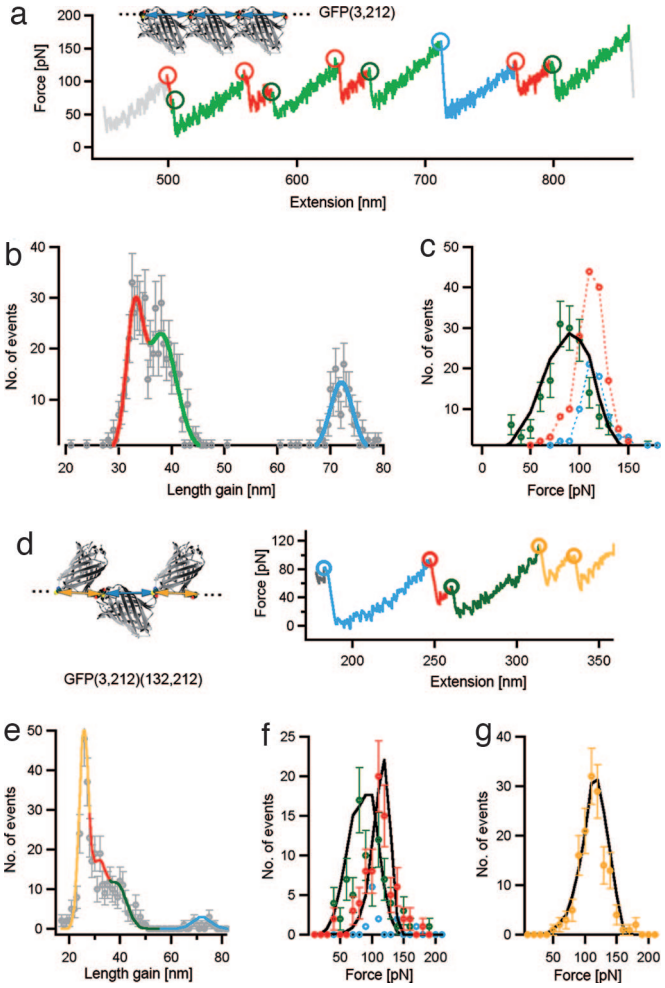

Fig. 4. Directional force application can populate a stable intermediate state. (*a*) Typical force-extension trace obtained with (3, 212)-linked GFP polyproteins. Blue, red, and green circles indicate complete GFP fracture, partial GFP fracture leading to the population of an intermediate state, and fracture of the intermediate state, respectively. (*b*) Contour length gain distribution (gray circles) obtained by fitting an interpolation of the WLC model (35) to individual peaks in the traces. Blue, red, and green solid lines indicate Gaussian fits to individual populations corresponding to complete GFP fracture, partial GFP fracture, and fracture of the intermediate state, respectively (compare, respectively, with the blue, red, and green sections in *a*). (*c*) Fracture force distribution for complete GFP fracture, partial GFP fracture, and fracture of the intermediate state (blue, red, and green circles, respectively), as identified by contour length increase. The black solid line indicates a simulated fracture force distribution that yields a potential width of 0.22 ± 0.01 nm and an unloaded transition rate of $6.5 \cdot 10^{-1} \pm 1\ s^{-1}$ for the intermediate state. (*d*) Typical force-extension trace obtained with GFP(3, 212)(132, 212) copolymerized proteins. The blue section indicates complete unfolding of GFP along (3, 212). The red section indicates partial unfolding of GFP along (3, 212). The green section indicates unfolding of the remaining intermediate along (3, 212). Yellow sections indicate two fracture events of GFP along (132, 212). (*e*) Contour length gain distribution for unfolding events in GFP(3, 212)(132, 212) copolymer force-extension traces. Four clearly separated peaks are visible: The yellow section matches unfolding of GFP along (132, 212), whereas the red, green, and blue sections reproduce the distribution shown in *b*. (*f*) Fracture force distribution for full fracture, partial fracture, and fracture of the intermediate state (blue, red, and green circles, respectively) of GFP(3, 212), as recorded with the copolymer. Black solid lines indicate a simulated fracture force distribution that yields the same potential width and transition rate for partial fracture of GFP(3, 212) as for the homopolymer (see Table 1) and a potential width of 0.22 ± 0.01 nm and an unloaded transition rate of $2 \times 10^{-1} \pm 1\ s^{-1}$ for the intermediate state. These values are consistent with the values obtained from the homopolymer. (*g*) Experimental and simulated fracture force distribution for unfolding of GFP(132, 212) (circles and black solid line) in the copolymer. Again, potential width and transition rates obtained from the copolymer are consistent with the values obtained in the homopolymer.

fracture should decrease with increasing number of unfolded domains within single force-extension traces because of the reduction in number of possible protein–protein interfaces. We do not observe such behavior (see the supporting information). To further investigate possible interface stabilization or aggregation effects, we constructed copolymers with mixed linkage geometries: (3, 212) and (132, 212). If interface interaction between neighboring units led to a stabilization of the intermediate state, a copolymer with mixed interfaces should greatly alter this effect. A zoom into a typical force-extension trace obtained with GFP(3, 212)(132, 212) copolymers exhibiting all classes of unfolding events is shown in Fig. 4*d*. A histogram of contour length increases for all observed events determined by fitting the WLC model to individual peaks in force-extension traces is shown in Fig. 4*e*. A comparison with Fig. 4*b* shows that copolymerization did not influence the apparent two-pathway unfolding behavior of GFP(3, 212). Fig. 4 *f* and *g* display fracture force distributions for the unfolding of GFP along the directions (3, 212) and (132, 212) in the copolymer, as identified by the contour length increases. All distributions can be well reproduced by using the same potential width and transition rates as in the respective homopolymers, providing evidence against stabilization effects coming from neighboring protein interfaces.

We therefore conclude that the GFP structure must contain two alternative pathways of similar stability along the (3, 212) deformation direction. The occurrence of a loading-direction-dependent intermediate structure shows that local minima of the energy landscape corresponding to partially folded structures so far inaccessible to experimental methods can now be populated and characterized (Fig. 1, pathway III).

Conclusions

In this study, we demonstrated how the energy landscape and three-dimensional deformation response of functional protein structures can be systematically explored by changing the direction of force application. A richness of behaviors with widely varying unfolding forces and various directional spring constants could be observed for the case of GFP, and a mechanical intermediate was found. Our results open the way to systematic toughness design of future protein-based materials (33).

Control over the sites of force application to single proteins also will offer unique possibilities to study enzyme function. The ability to sense conformational changes of a working enzyme at predefined contact points will be an important application of single-molecule mechanics in the future.

Materials and Methods

Construction of GFP Polyproteins. Pairwise point mutations of wild-type GFP residues Lys3Cys, Asp117Cys, Glu132Cys, Tyr182Cys, and Asn212Cys were performed with a QuikChange multisite directed mutagenesis kit (Stratagene). Purification of the His_6-tagged proteins was done with Ni-NTA affinity chromatography at 4°C. All GFP double-cysteine mutants showed typical, bright GFP fluorescence, indicating the presence of the native GFP structure. Polymerization of GFP double-cysteine mutants was performed in PBS buffer, pH = 7.4 at a protein concentration of ≈0.2 mM. Saw-tooth patterns in force spectroscopy data confirmed the presence of long polymers after incubation for 80 h at 37°C for samples GFP(3, 132), GFP(3, 212), GFP(132, 212), and GFP(182, 212). We incubated GFP(117, 182) at 37°C for 10 days to obtain long polymers. Samples were then stored at 4°C to slow down further polymerization. For copolymerization of the variants GFP(3, 212) and GFP(132, 212), we first reduced the linking disulfide bonds by applying 20 mM DTT to the polymerized sample solutions, followed by mixing the resulting monomeric sample solutions in a 1:1 concentration ratio. We then exchanged buffer to remove all traces of DTT by using twice HiTrap desalting columns (GE

Healthcare, Munich, Germany). Subsequent incubation at 37°C for ≈80 h lead then to copolymers confirmed by the appearance of both GFP(3, 212) and GFP(132, 212) unfolding patterns in the same single-molecule force-extension traces (see Fig. 4). See ref. 34 for a detailed cysteine engineering protocol.

Single-Protein Force Spectroscopy. All single-molecule force measurements were performed on a custom-built atomic force microscope at room temperature. Gold-coated cantilevers (BioLevers; Olympus, Tokyo, Japan) with spring constant and resonance frequency of 30 pN/nm and 8.5 kHz (type A) were used. For the measurements, protein solutions were centrifuged at 10,000 × *g* in a tabletop centrifuge to spin-down possible larger aggregates. Ten microliters of protein solution was applied to a glass surface [GFP(117, 182) and GFP(182, 212) were applied to a gold-evaporated glass surface] and incubated for 60 min at room temperature. All force traces were collected at a pulling speed of 3.6 μm/s except the traces on GFP(3, 132). Unfolding forces were determined by taking the force peak value for each individual unfolding event in single-molecule traces. GFP(3, 132) polyproteins were further investigated at two different pulling speeds (2 μm/s and 12 μm/s) to check for any unexpected pulling speed dependence, which we did not observe.

Contour Length Measurements. WLC force-extension traces were calculated by using the interpolation formula $F(x) = (k_BT/p)[0.25(1 - x/L)^{-2} - 0.25 + x/L]$ (35) and fit to individual peaks in the experimental force-extension traces. L denotes contour length, p is persistence length, k_B is Boltzmann's constant, T is temperature, and x is the distance between attachment points of the proteins. We used $p = 0.5$ nm for fitting the data collected on GFP(3, 212), GFP(132, 212), and the copolymer *GFP*(3, 212)(132, 212) in a force range of 50–150 pN (36). $p = 0.35$ nm was used for fitting the GFP(182, 212), GFP(117, 182), and GFP(3, 132) data in the force range above 150 pN (6).

Monte Carlo Simulations. To interpret the distributions of observed unfolding forces, we performed Monte Carlo simulations as described previously (26). Experimental conditions were simulated by including the measured distribution of contour lengths at which the first of a series of unfolding events was observed and by including the distribution of the number of monomers unfolded in each measured trace. For a given set of parameters, we averaged 30 simulated unfolding force distributions and fitted to those obtained experimentally to yield the (unloaded) natural transition rate $k_{i,j}(F = 0)$ under zero force and $\Delta x_{i,j}$, which denotes the distance from the folded state to the transition state (termed "potential width" in the text) along the direction defined by the points of force application.

Estimating Transition Barrier Heights and Directional Spring Constants. The activation barrier height $\Delta G^*_{i,j}$ was calculated by using the Arrhenius equation $\Delta G^*_{i,j} = -k_BT \cdot \ln(k_{i,j}/k_A)$, where $k_{i,j}$ denotes the unloaded transition rate in direction (i, j) and k_A is the Arrhenius frequency factor. For protein dynamics, k_A has a value of 10^9 s^{-1} (37). We chose this value for all barrier height estimations. To estimate an elastic spring constant $p_{i,j}$ of the folded protein structure along a certain direction, we assumed harmonic potentials, hence $p_{i,j} = 2 \cdot \Delta G^*_{i,j}/\Delta x_{i,j}^2$, where $\Delta x_{i,j}$ denotes the potential width along direction (i, j).

This work was supported by Deutsche Forschungsgemeinschaft Grant SFB413.

1. Bustamante, C., Chemla, Y. R., Forde, N. R. & Izhaky, D. (2004) *Annu. Rev. Biochem.* **73,** 705–748.
2. Pauling, L. (1946) *Chem. Eng. News* **24,** 1375–1377.
3. Rief, M., Gautel, M., Schemmel, A. & Gaub, H. E. (1998) *Biophys. J.* **75,** 3008–3014.
4. Tskhovrebova, L., Trinick, J., Sleep, J. A. & Simmons, R. M. (1997) *Nature* **387,** 308–312.
5. Kellermayer, M. S., Smith, S. B., Granzier, H. L. & Bustamante, C. (1997) *Science* **276,** 1112–1116.
6. Carrion-Vazquez, M., Marszalek, P. E., Oberhauser, A. F. & Fernandez, J. M. (1999) *Proc. Natl. Acad. Sci. USA* **96,** 11288–11292.
7. Carrion-Vazquez, M., Oberhauser, A. F., Fowler, S. B., Marszalek, P. E., Broedel, S. E., Clarke, J. & Fernandez, J. M. (1999) *Proc. Natl. Acad. Sci. USA* **96,** 3694–3699.
8. Cecconi, C., Shank, E. A., Bustamante, C. & Marqusee, S. (2005) *Science* **309,** 2057–2060.
9. Oesterhelt, F., Oesterhelt, D., Pfeiffer, M., Engel, A., Gaub, H. E. & Muller, D. J. (2000) *Science* **288,** 143–146.
10. Muller, D. J., Kessler, M., Oesterhelt, F., Moller, C., Oesterhelt, D. & Gaub, H. (2002) *Biophys. J.* **83,** 3578–3588.
11. Kedrov, A., Ziegler, C., Janovjak, H., Kuhlbrandt, W. & Muller, D. J. (2004) *J. Mol. Biol.* **340,** 1143–1152.
12. Kessler, M., Gottschalk, K. E., Janovjak, H., Muller, D. J. & Gaub, H. E. (2006) *J. Mol. Biol.* **357,** 644–654.
13. Carrion-Vazquez, M., Li, H., Lu, H., Marszalek, P. E., Oberhauser, A. F. & Fernandez, J. M. (2003) *Nat. Struct. Biol.* **10,** 738–743.
14. Brockwell, D. J., Paci, E., Zinober, R. C., Beddard, G. S., Olmsted, P. D., Smith, D. A., Perham, R. N. & Radford, S. E. (2003) *Nat. Struct. Biol.* **10,** 731–737.
15. Navizet, I., Cailliez, F. & Lavery, R. (2004) *Biophys. J.* **87,** 1426–1435.
16. Dietz, H. & Rief, M. (2006) *Proc. Natl. Acad. Sci. USA* **103,** 1244–1247.
17. Onuchic, J. N. & Wolynes, P. G. (2004) *Curr. Opin. Struct. Biol.* **14,** 70–75.
18. Murzin, A. G., Brenner, S. E., Hubbard, T. & Chothia, C. (1995) *J. Mol. Biol.* **247,** 536–540.
19. Fukuda, H., Arai, M. & Kuwaijima, K. (2000) *Biochemistry* **39,** 12019–12024.
20. Helms, V., Straatsma, T. P. & McCammon, J. A. (1999) *J. Phys. Chem. B* **103,** 3263–3269.
21. Zimmer, M. (2002) *Chem. Rev.* **102,** 759–781.
22. Dietz, H. & Rief, M. (2004) *Proc. Natl. Acad. Sci. USA* **101,** 16192–16197.
23. Rief, M., Gautel, M., Oesterhelt, F. Fernandez, J. M. & Gaub, H. E. (1997) *Science* **276,** 1109–1112.
24. Marszalek, P. E., Lu, H., Li, H., Carrion-Vazquez, M., Oberhauser, A. F., Schulten, K. & Fernandez, J. M. (1999) *Nature* **402,** 100–103.
25. Rounsevell, R. W., Steward, A. & Clarke, J. (2005) *Biophys. J.* **88,** 2022–2029.
26. Rief, M., Fernandez, J. M. & Gaub, H. E. (1998) *Phys. Rev. Lett.* **81,** 4764–4767.
27. Zinober, R. C., Brockwell, D. J., Beddard, G. S., Blake, A. W., Olmsted, P. D., Radford, S. E. & Smith, D. A. (2002) *Protein Sci.* **11,** 2759–2765.
28. Grandbois, M., Beyer, M., Rief, M., Clausen-Schaumann, H. & Gaub, H. E. (1999) *Science* **283,** 1727–1730.
29. Evans, E. & Ritchie, K. (1997) *Biophys. J.* **72,** 1541–1555.
30. Schlierf, M. & Rief, M. (2005) *J. Mol. Biol.* **354,** 497–503.
31. Tajkhorshid, E., Aksimentiev, A., Balabin, I., Gao, M., Isralewitz, B., Phillips, J. C., Zhu, F. & Schulten, K. (2003) *Adv. Protein Chem.* **66,** 195–247.
32. Grubmuller, H. (2005) *Methods Mol. Biol.* **305,** 493–515.
33. Smith, B. L., Schäffer, T. E., Viani, M., Thompson, J. B., Frederick, N. A., Kindt, J., Belcher, A., Stucky, G. D., Morse, D. E. & K., H. P. (1999) *Nature* **399,** 761.
34. Dietz, H., Bertz, M., Schlierf, M., Berkemeier, F., Bornschlogl, T., Junker, J. & Rief, M. (2006) *Nat. Protocols* **1,** 80–84.
35. Bustamante, C., Marko, J. F., Siggia, E. D. & Smith, S. (1994) *Science* **265,** 1599–1600.
36. Schwaiger, I., Kardinal, A., Schleicher, M., Noegel, A. A. & Rief, M. (2004) *Nat. Struct. Mol. Biol.* **11,** 81–85.
37. Bieri, O., Wirz, J., Hellrung, B., Schutkowski, M., Drewello, M. & Kiefhaber, T. (1999) *Proc. Natl. Acad. Sci. USA* **96,** 9597–9601.
38. Brejc, K., Sixma, T. K., Kitts, P. A., Kain, S. R., Tsien, R. Y., Ormo, M. & Remington, S. J. (1997) *Proc. Natl. Acad. Sci. USA* **94,** 2306–2311.